IRIS AperTO

UNIVERSITÀ DEGLI STUDI DI TORINO

AperTO - Archivio Istituzionale Open Access dell'Università di Torino

Discovering connections between terahertz vibrations and elasticity underpinning the collective dynamics of the HKUST-1 metal-organic framework

This is a pre print version of the following article:

Original Citation:

Availability:

This version is available http://hdl.handle.net/2318/1622801 since 2021-03-24T19:50:14Z

Published version:

DOI:10.1039/c5ce02347e

Terms of use:

Open Access

Anyone can freely access the full text of works made available as "Open Access". Works made available under a Creative Commons license can be used according to the terms and conditions of said license. Use of all other works requires consent of the right holder (author or publisher) if not exempted from copyright protection by the applicable law.

(Article begins on next page)

12 October 2024

Discovering connections between Terahertz vibrations and elasticity underpinning the collective dynamics of HKUST-1 metal-organic framework

Matthew R. Ryder,[a,b] Bartolomeo Civalleri,[c] Gianfelice Cinque[b] and Jin-Chong Tan[a*]

We employed a combination of theoretical and experimental techniques to study the metal-organic framework (MOF)-mechanics central to the paddle-wheel $Cu_3(BTC)_2$ porous structure, commonly designated as HKUST-1. Lattice dynamics of the hybrid framework at below 18 THz were measured by means of Raman and synchrotron far-infrared spectroscopy, and systematically correlated to collective vibrational modes computed from *ab initio* density functional theory (DFT). We have identified a number of intriguing low-energy framework vibration mechanisms, reminescent of the 'trampoline-like' deformations and new oscillatory motions associated with Cu paddle-wheel 'molecular rotors'. The three independet elastic constants of the HKUST-1 single crystal (i.e. C_{11}, C_{12} and C_{44}) were calculated using the DFT approach, taking into account the effects of dispersion corrections. We established the full elasticity solutions accompanying detailed deformation mechanisms that control its anisotropic mechanical properties, ranging from the Young's and shear moduli to linear compressibility and Poisson's ratio. Our results support the notion that the co-existance of soft modes and intrinsic shear distortions connected to the THz lattice dynamics dictate anomalous elastic phenomena, for exemplar: negative Poisson's ratio (auxeticity), negative thermal expansion (NTE), and exceedingly low shear moduli property.

1. Introduction

Metal-organic frameworks (MOFs)[1] are contemporary nanoporous solids with vast structural versatility,[2] giving rise to highly tunable physical and chemical functionalities.[3] The current trend is rapidly shifting from purely chemical structures discovery to development of potential applications to afford commercial use in industry, engineering, and value-added products.[4] In fact, research into potential applications of MOFs are no longer limited to gas separations, carbon capture and adsorption,[5] but expanding into many innovative domains encompassing optoelectronics[6] and lighting,[7] biomedicine,[8] heterogeneous catalysis[9] and chemical sensing.[10]

The basic mechanical properties[11-13] and material toughness,[14, 15] in conjunction with long-term structural, moisture and chemical stability of MOFs are central for manufacturing,[16] shaping[17] and scaling up, all of which underpinning successful deployment of aforementioned applications in many diverse technological settings. The emerging field of "MOF-mechanics",[13, 18, 19] particularly concerning the effects of elevated pressure (i.e. hydrostatic compression) on the structural transformation and chemical response of MOFs is an area of intense study.[20, 21] Tunability of MOF mechanical properties made possible through isoreticular design and construction,[22] host-guest interactions,[23] and chemical modification[24] is another topic of current interest. Given the flexible nature of open frameworks[25] attributed to compliant metal coordination environments bridged by organic linkages, they offer exciting new opportunities to yield unusual elastic response (*i.e.* mechanical metamaterials)[26] which are rare in conventional materials, for example: negative linear compressibility (NLC), negative Poisson's ratio (NPR or auxeticity), and negative thermal expansion (NTE).[18, 19, 21] Large elastic anisotropy of MOFs are notable,[18, 27] and this property could have important consequences on both mechanical and thermal stability determining the robustness of porous framework against structural destabilization,[28] irreversible plastic deformation[11, 29] and amorphization.[30]

Low-frequency lattice modes — called "Terahertz (THz) vibrations"[31] have recently been demonstrated to be prevalent in the family of zeolitic MOFs.[32] These collective modes detected at THz frequencies have been identified to have a major influence for triggering a range of intriguing lattice dynamics, particularly gate opening and breathing phenomena dictating influx and release of absorbents, soft modes and shear-induced deformations that might be the source of framework destabilization and collapse. While the structural dynamics of certain MOFs have been studied before,[33] there is no detailed work connecting the behaviour of THz dynamics and elastic anisotropy to facilitate understanding of basic core mechanisms of MOFs. In this paper, we described the use of

[a.] *Department of Engineering Science, University of Oxford, Parks Road, Oxford OX1 3PJ, UK*
[b.] *Diamond Light Source, Harwell Campus, Didcot, Oxford OX11 0DE, UK*
[c.] *Department of Chemistry, NIS and INSTM Reference Centre, University of Turin, via Pietro Giuria 7, 10125 Torino, Italy*
**Corresponding author: jin-chong.tan@eng.ox.ac.uk*

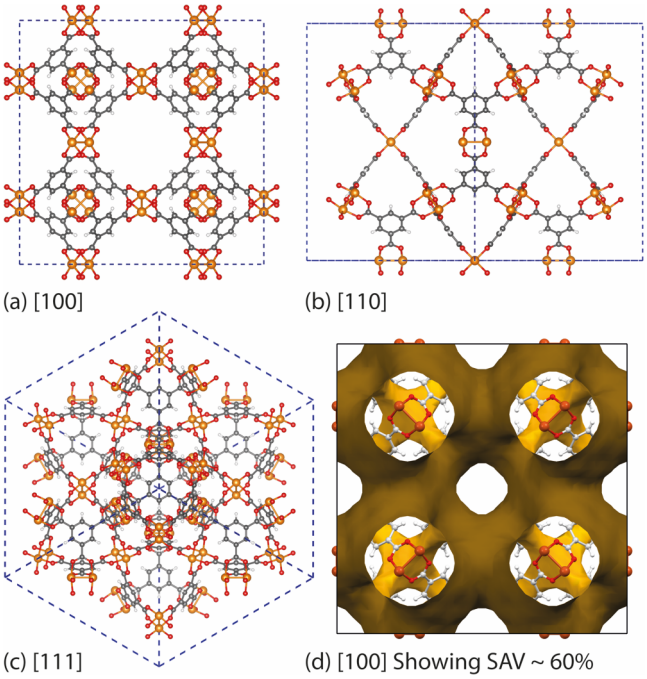

Fig. 1 Crystal structure of HKUST-1 looking down the (a) <100>, (b) <110> and (c) <111> directions and (d) <100> direction displaying the Solvent Accessible Volume (SAV). Colour code used: copper, orange; carbon grey; oxygen red; hydrogen white.

Raman and synchrotron far-infrared spectroscopy techniques in combination with *ab initio* density functional theory (DFT), to pinpoint and elucidate low-energy vibrational modes and associated deformation mechanisms detected in the paddle-wheel HKUST-1 [$Cu_3(BTC)_2$; BTC = benzene-1,3,5-tricarboxylic acid][34] porous framework structure (Fig. 1).

2. Experimental & theoretical methods

2.1 Experimental methodology

Infrared (IR) absorption spectra of HKUST-1 was recorded at the Multimode InfraRed Imaging and Microspectroscopy (MIRIAM) Beamline B22 at Diamond Light Source. The beamline was in 'standard mode', hence 900 bunches filling pattern for a total circulating current of 300 mA with top-ups every 10 mins (with a lifetime of 18 hours). The spectrum was obtained under vacuum using a Bruker Vertex 80V Fourier Transform Infrared (FTIR) interferometer equipped with a DTGS detector with a resolution of 1 cm^{-1} and utilising a 6 µm Mylar broad-band multilayer beamsplitter. The specific beamsplitter used allowed for excellent spectra to be obtained in the region < 600 cm^{-1} (18 THz) In addition, the data was recorded at room temperature *via* an Attenuated Total Reflection (ATR) method. Specifically, HKUST-1 powder was placed on top of a diamond ATR crystal and held in position by pressure applied on a high density polyethylene (HDPE) disk. The IR beam therefore enters the ATR crystal from the bottom at an angle of 45° and is totally reflected at the interface of the crystal and the sample, then redirected by a 45° mirror to a detector.

Raman spectra was recorded using a Bruker Senterra confocal instrument with a 50x microscope operating with a 532 nm laser, with a 50 micron aperture setting and a 1% optical filter.

Computational Methodology

We performed *ab initio* density functional theory (DFT) calculations using the periodic code CRYSTAL14.[35] Gaussian-type atom-centred all-electron basis sets were used consisting of 2,880 basis functions for all of the HKUST-1 calculations. The geometry was optimised at the B3LYP and B3LYP-D levels of theory by relaxation of both the lattice parameters and atomic coordinates. To ensure the optimised structures were accurate the convergence criteria of the route mean square (RMS) of the gradient and the displacement were increased, from the default values of 0.0003 a.u. and 0.0012 a.u. to 0.0002 a.u. and 0.0004 a.u., respectively. In addition, the self-consistent field (SCF) convergence threshold was also improved from 10^{-7} a.u. to 10^{-10} a.u on the total energy and tighter tolerances for the evaluation of two-electron integrals were used.

The single-crystal elastic constants of the elasticity matrix (tensor) were calculated using the numerical first derivative of the analytic cell gradients.[36] These values correspond to the independent elastic stiffness coefficients, C_{ij}.[37] The unique coefficients were obtained *via* the method of deforming the optimised structure, using a three-point formula, in the symmetrically required directions of both positive and negative amplitudes. These particular deformations correspond to tensile and compressive strains required to obtain the elastic response. The magnitude of each individual strain deformation is defined as 1%, ensuring the response is in the purely elastic region. The mechanical properties were calculated *via* tensorial analysis implemented in Mathematica[38] and the ElAM code.[39]

The vibrational frequencies at the gamma point were obtained by slightly displacing the optimised structure, with respect to the 3N atomic coordinated, to allow for numerical differentiation of the analytical first derivatives, hence producing the mass-weighted Hessian matrix.[40] The intensities of the IR-active modes were calculated *via* numerical differentiation, using the Berry phase approach.[41] More specifically, the atomic Born tensors were evaluated *via* the derivation of the dipole moment with respect to the atomic displacements. This equates to the polarization differences between the optimised and the displaced structures and is equivalent to the time-integrated transient current that flows through the material during the vibrations. The intensities of the Raman-active modes were calculated analytically via Coupled Perturbed Hartree-Fock (CPHF) theory[42] and corrected for the experimental parameters of a laser frequency of 532 nm and a temperature of 293 K.

TABLE 1. Notable collective vibrational modes of HKUST-1

Mode (cm^{-1})	(THz)	Activity	IRREP*	Description
16.32	0.49	Non	F_{2u}	Strong Paddle Wheel Deformation and Translational Motion (Symmetric Cluster Rotation)
20.43	0.61	Non	E_u	Strong Paddle Wheel Deformation and Translational Motion
58.07	1.74	Raman	F_{2g}	Strong Paddle Wheel Rotation with Organic Linker Trampoline-like Motion
63.17	1.89	Non	F_{2u}	Paddle Wheel Deformation and Translational Motion with Organic Linker Rotating
78.28	2.35	Non	B_g	Paddle Wheel Deformation with Organic Linker Rotating (Symmetric Cluster Rocking)
81.47	2.44	IR	F_{1u}	Organic Linker Trampoline-like Motion
94.15	2.82	Non	B_u	Organic Linker Trampoline-like Motion
98.41	2.95	Raman	A_g	Organic Linker Trampoline-like Motion (Symmetric Cluster Breathing)

*IRREP = Irreducible representation; Non = non-optically active mode

3. Results and discussion

3.1 Vibrational motions present in HKUST-1

The vibrational modes located in the mid-infrared (MIR) region are simply due to the common chemical vibrational motions of any system containing organic moieties. These motions are well characterised and understood and are the result of bond stretching and bending. Even in hybrid materials, such as MOFs, the variations from the isolated organic linkers are minor. However, the low energy vibrations located in the far-infrared (FIR) region are not as trivial to explain, and this is due to them no longer originating from isolated molecular motions but instead involve the collective motion of the framework (lattice vibrations).[32] In HKUST-1, particularly interesting lattice vibrations were detected to lie in the region of under 600 cm^{-1} (<18 THz) and involve contributions varying from Cu-paddle-wheel deformations, indicative of possible molecular rotor potentials,[43] to organic linker movements which could explain the phenomenon of negative thermal expansion (NTE) experimentally confirmed in HKUST-1.[44]

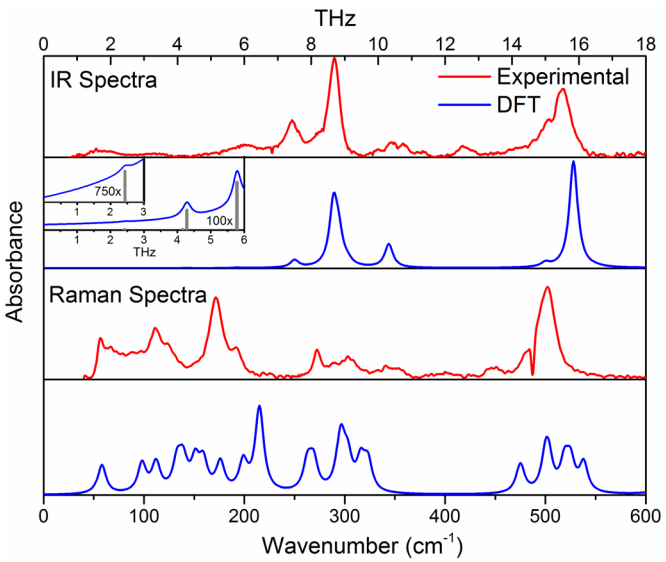

Fig. 2 Comparison of experimental and theoretical Far-infrared (FIR) and Raman spectra in the 0–600 cm^{-1} (0-18 THz) region. An empirical 10 cm^{-1} FWHM Lorentzian line shape was applied to the DFT spectra to aid in comparison to the FIR data and a bar representation is present for the low intensity IR region below 6 THz.

Herein we have compared the experimental and theoretical IR-active and Raman-active vibrational motions identified in the region less than 18 THz. As can be seen from Fig. 2, the agreement is very good for both IR and Raman spectra. To gain a full physical understanding of the lattice dynamics of HKUST-1, we calculated the theoretical vibrational spectra using DFT, at the B3LYP level of theory with and without corrections for dispersion. Due to the high cubic symmetry present in HKUST-1 there are not that many unique vibrational modes in this important region, specifically we determined respectively 12 and 25 unique IR and Raman active motions located under 600 cm^{-1}. It is worth mentioning, however, that many of the modes are triply degenerate, due to the symmetry of the framework and in addition, there are also 44 unique non-optically active vibrational motions in the same spectral region. In the next section, we will summarise all of the IR and Raman active modes and highlight some of the non-optically active modes that are of significant interest to the framework elastic properties and its anisotropy discussed after.

3.2 Distinct regions of THz vibrational modes of HKUST-1

Altogether HKUST-1 has 81 unique vibrational motions located under 600 cm^{-1}, all of which are summarised in the ESI. The majority are due to the deformational movements of either the organic linker moieties or the inorganic Cu-centric paddle wheel units but can be grouped into distinctive spectral regions, and there are many interesting motions located in the low-energy region under 100 cm^{-1}. Specifically, the vibrational modes can be characterised into the following regions, working from the higher energy modes downwards:

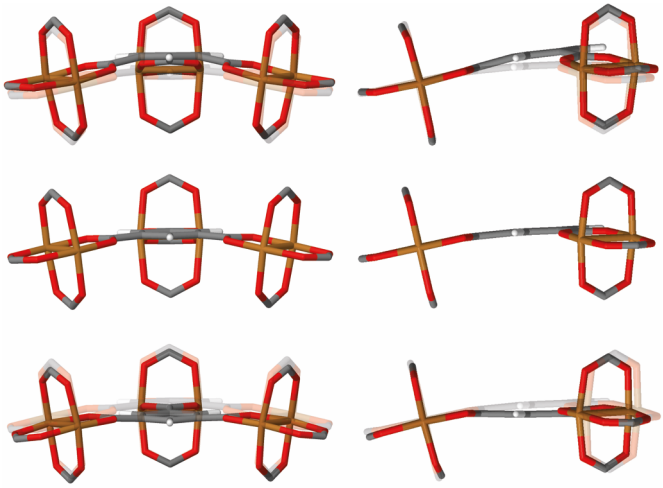

(a) <111> View (b) <110> View

Fig. 3 Low energy collective vibration, located at 81 cm^{-1} (2.4 THz), viewed down the (a) <111> and (b) <110> directions, showing a 'trampoline-like' motion linked to negative thermal expansion (NTE). Videos of the motions are available in the ESI.

- Above 530 cm^{-1} (> 16 THz) are Cu-O stretching motions;
- Modes lying within 400-530 cm^{-1} (*ca*. 12-16 THz) are in-plane and out-of-plane aromatic ring deformations;
- 100-400 cm^{-1} modes (*ca*. 3-12 THz) are various combinations of 'paddle-wheel' deformations and linker rotational motions. These oscillatory deformations mainly consist of Cu-O stretching, O-Cu-O bending, and an interesting Cu-Cu buckling motion similar to vibrational buckling motions in small organic molecules.[45] Another interesting observation in this region, are modes where the symmetry of the displacements result in a swelling or 'breathing' appearance of the Cu-based paddle-wheel unit. These particular motions are all Raman-active and located around 3.4 and 6.4 THz, (112, 214 and 215 cm^{-1}), with the lowest energy example exhibiting the strongest structural deformation effect;
- Modes under 100 cm^{-1} (< 3THz) are associated with collective framework vibrations, including 'trampoline-like' motions, paddle-wheel rotors, and symmetric collective motions that could explain the source of anomalous mechanical behaviour.

3.3 Noteworthy collective vibrations

We have discovered 8 unique collective vibrations of significant interest each originating from three specific classes of motion. The first interesting motion can be described as 'trampoline-like' deformation and is depicted in Fig. 3. There are four vibrational modes demonstrating this particular motion, located at 58, 81, 94 and 98 cm^{-1} (from 1.7 to 3 THz) corresponding to the Raman, IR, non-optically active, and Raman-active modes, respectively. The IR and non-active motions are primarily just the movement of the organic linker in a trampoline-like fashion but the Raman-active ones are more distinct. This is due to the symmetry of the mode located at 98 cm^{-1}, resulting in a breathing effect of the organic-inorganic cluster. In addition, the lower-energy Raman active mode at 58 cm^{-1} also shows the second class of motion, involving a rotation of the paddle-wheel unit simultaneously. This particular combination of motions are analogous to modes that have been suggested experimentally to drive negative thermal expansion (NTE).[44] The previous work[44] showed thermal ellipsoids suggesting the 'trampoline-like' motion at a temperature range of 100-404 K and also proposed that the liberation of the aromatic rings and twisting of the 'paddle-wheel' unit also contribute to the expansion upon thermal stimulus.[44] All of these low-energy deformation have been demonstrated in full in our work, with the indication that NTE can be driven by a combination of THz vibrational motions. Such NTE phenomenon is possibly including the other non-active modes (located at 16, 20, 63 and 78 cm^{-1}), showing translational and rotating motions of the organic linker and Cu-based paddle-

TABLE 2. Single-crystal elastic stiffness coefficients (C_{ij}) of HKUST-1 computed from the DFT method

Functional	C_{11}	C_{12}	C_{44}
B3LYP	27.719	25.722	5.399
B3LYP-D	27.539	25.476	5.273

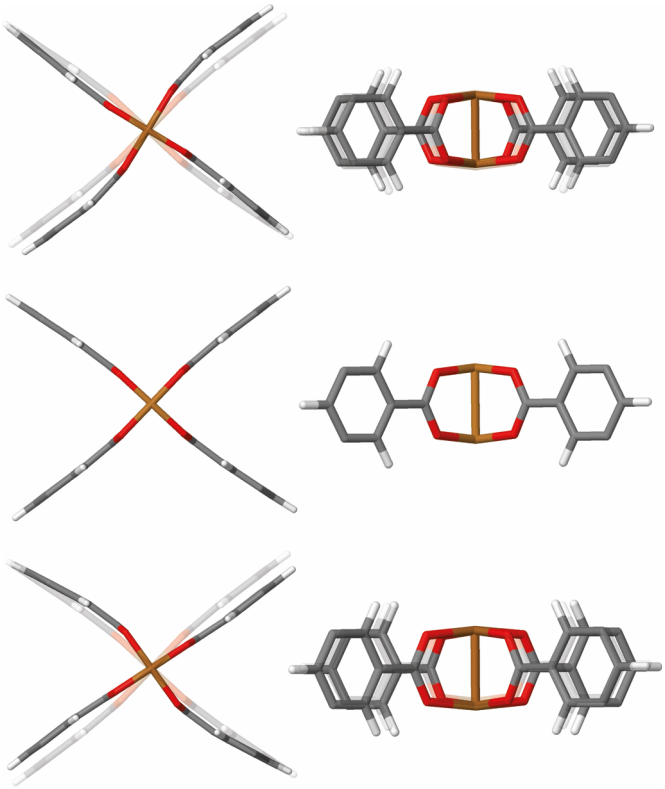

(a) <110> View (b) <011> View

Fig. 4 Low energy collective vibration, located at 58 cm^{-1} (1.7 THz), viewed down the (a) <110> and (b) <011> directions, showing a rotor motion of the Cu-based paddle-wheel moiety. Videos of the motions are available in the ESI.

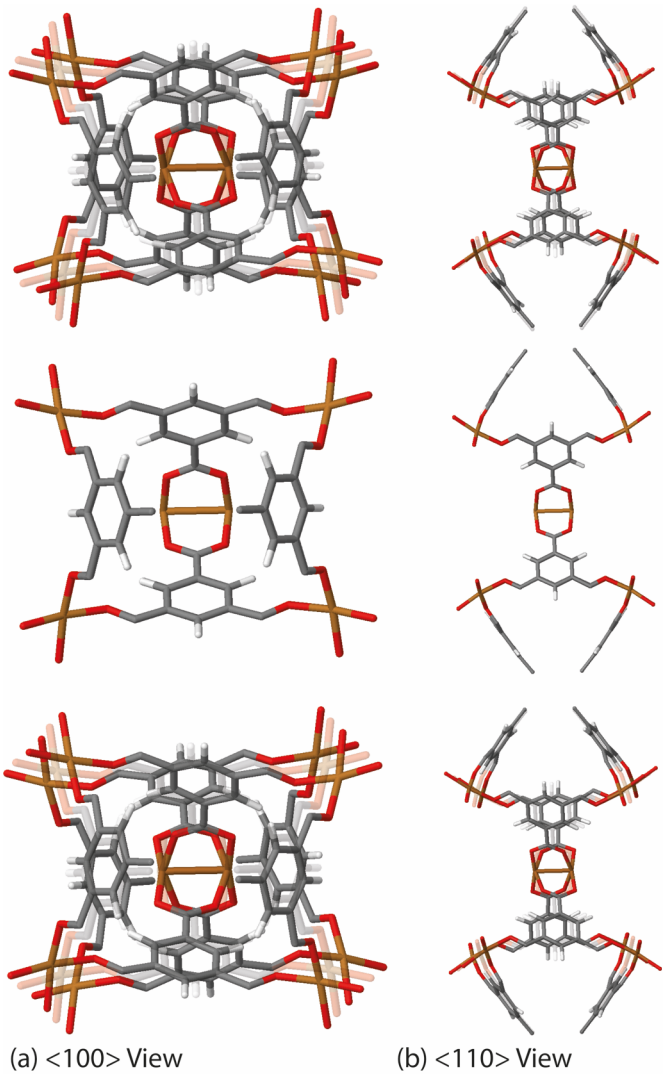

Fig. 5 Low energy collective vibration, located at 16 cm^{-1} (0.5 THz), viewed down the (a) <100> and (b) <110> directions, showing a cluster rotation mechanism, linked to auxeticity. Videos of the motions are available in the ESI.

wheel which are all located in the important low-energy (THz) region, see summary in Table 1. It is also worth noting that similar motions have been suggested to be the source of NTE in other less complex MOF materials, such as the cubic MOF-5.[46]

The second intriguing class of collective dynamics already mentioned above is the strong paddle-wheel rotor shown to be linked to the Raman-active mode at 58 cm^{-1} (1.7 THz). This particular motion is of high interest as it could suggest the possibility of utilising the mechanism for potential 'molecular' rotor applications.[47] This is a topical area of research with some examples in MOFs starting to appear.[43, 48] However, most work done on MOFs has concentrated on the use of the organic linkers which is dissimilar from the rotation attributed to the metal-containing units, such as the rotor dynamics identified here regarding the paddle-wheel of HKUST-1.

The final exciting vibrational motion revealed from our work is less trivial to describe in words, but videos of its structural dynamics can be seen in the ESI to aid in the conceptualisation. In principle, the motions fully involve the collective framework and the organic-inorganic cluster, briefly mentioned when discussing the Raman-active mode at 98 cm^{-1} (~3 THz). There are other modes in HKUST-1 whose dynamics are reminiscent of this motion, although they are more due to the symmetry of the mode resulting in the effect of cluster movement. Examples other than the Raman-active mode discussed, are a non-active cluster rocking motion located 78 cm^{-1} (2.3 THz) and this is accompanied by another non-active higher energy cluster rocking motion at 138 cm^{-1} (~4 THz). However, the most exciting cluster-linked motion is the non-active mode at 16 cm^{-1}, which is the lowest energy vibrational mode of HKUST-1 found at *ca.* 0.5 THz. This particular motion involves a combination of rocking and translational dynamics resulting in the rotation of the linker-paddle-wheel 4-noded cluster. The rotational movement of the cluster could reveal the nature of the mechanism behind anomalous elastic behaviour present in the material, specifically the directional auxetic response (negative Poisson's ratio), discussed in more detail later in this work.

3.4 Single-crystal elastic constants of HKUST-1

The vibrational motions discussed so far can be intrinsically linked to the mechanical behaviour of HKUST-1, especially its elastic response. We therefore, have calculated the single-

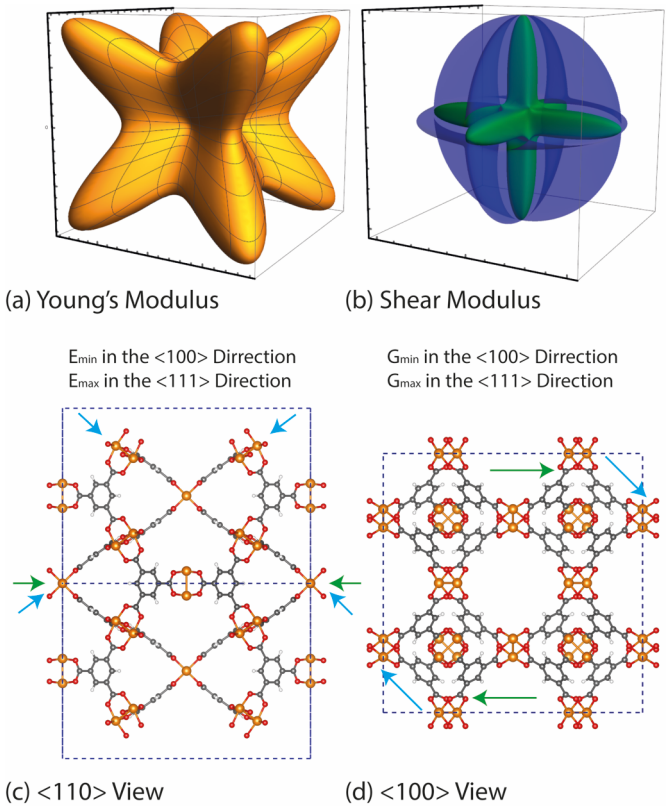

Fig. 6 (a) Young's modulus representation surface $E(\vartheta, \varphi)$ in 3-D spherical coordinates, along with (b) shear modulus representation surface $G(\vartheta, \varphi, \chi)$. The accompanying structure-property relationships can be seen for (c) E_{min} is along the <100> axes and E_{max} is along the <111> axes. (d) G_{min} is along the <100> axes and G_{max} is along the <111> axis.

crystal elastic constants using DFT and *via* tensorial analysis can obtain the related mechanical properties, i.e. Young's modulus, shear modulus, linear compressibility and Poisson's ratio. The link between the elastic constants and the mechanical response is from Hooke's law being related to stress σ and strain ε (both second-rank tensors) in the following equation:[37]

$$\sigma_{ij} = \sum_{kl} C_{ijkl}\varepsilon_{kl}$$

where C_{ijkl} represents the symmetric fourth-rank elasticity tensor connecting stress to strain. HKUST-1 only has three unique elastic constants (see Table 2), due to having a cubic symmetry and the symmetric elasticity matrix (stiffness tensor) therefore is:

$$C_{cubic} = \begin{pmatrix} C_{11} & C_{12} & C_{12} & 0 & 0 & 0 \\ & C_{11} & C_{12} & 0 & 0 & 0 \\ \vdots & & C_{11} & 0 & 0 & 0 \\ & & & C_{44} & 0 & 0 \\ & \iddots & & & C_{44} & 0 \\ \text{symm.} & & \dots & & & C_{44} \end{pmatrix}$$

The diagonal coefficient C_{11} represents the framework stiffness along each of the three principal crystal axes, *i.e.* a, b, and c (due to them being equal) under uniaxial strain. The other diagonal coefficient C_{44} is the shear stiffness measuring angular distortion against a shear deformation. The off-diagonal coefficient C_{12} signifies the tensile-tensile coupling between any two orthonormal axes. Importantly, the mechanical properties discussed in the next section are calculated from the inversion of the elasticity matrix, known as the compliance matrix (S) in accordance to:

$$S_{ijkl} = C_{ijkl}^{-1}$$

3.5 Framework elastic anisotropy under uniaxial and angular deformations

The elastic anisotropy of HKUST-1 can be witnessed when examining the 3-D directional Young's and shear moduli (see Fig. 6 and Table. 2). Firstly the Young's modulus is simply the ratio of uniaxial stress over strain and can be obtained via tensorial analysis of the compliance matrix through the following equation, depending on a unit vector **u**:

$$E(\mathbf{u}) = \frac{1}{u_i u_j u_k u_l S_{ijkl}}$$

Both the minimum and maximum Young's moduli of HKUST-1 can be easily explained from a structure-property relationship. The origin of E_{max} (15 GPa) is related to compression in the direction of the planarity of the aromatic rings. The link between deforming aromatic rings of the organic linker and the direction of E_{max} has also been recently reported for ZIF and MIL structures.[18] [?] In the case of HKUST-1 these maxima are located along the [111] axes. Another intriguing uniaxial property is the minimum Young's moduli, E_{min} (see Fig. 6). The minimum is located along the [001] axes and can be related to only partial reinforcement of the linker-paddle-wheel-linker (L-PW-L) moiety oriented along each axes. The L-PW-L unit does not provide as much mechanical rigidity as the single-linker reinforcement that has been recently demonstrated in our work on the Zr-based MIL-140 series and hence we see an E_{min} of just 3 GPa.[?]

Moving on to the angular rigidity of HKUST-1, we evaluate the shear modulus which can similarly be straightforwardly explained *via* structure-property relationships. Unlike the uniaxial directions of the 3-D Young's modulus surface, the shear modulus depends on an additional unit vector **v** and hence the representation shown in Fig. 6, depicts the maximum (blue) and minimum response (green) resulting from angular deformations in the respective directions. As per the single unit vector equation shown earlier, the shear modulus is also derived from the compliance matrix but via the following two unit vector equation:

$$G(\mathbf{u}, \mathbf{v}) = \frac{1}{u_i v_j u_k v_l S_{ijkl}}$$

Due to the cubic symmetry the maximum and minimum values (G_{max} and G_{min}) are located in multiple directions, with G_{max} lying along each principal crystallographic axes [100] whereas G_{min} present in the [111] direction. This logically is due to the nodes inclusive of flexible organic components allowing for deformation upon shear strain more easily than the inorganic-based paddle-wheel on its own. This effect is illustrated very clearly in Fig. 6, where the different nodes are highlighted.

Before moving on to more complex elastic behaviour, it is worth noting that due to the cubic space group of HKUST-1, the linear compressibility (β) response of the framework upon hydrostatic compression is isotropic, unlike all of the other mechanical properties discussed in this work. The magnitude of

TABLE 2. Mechanical properties of HKUST-1

Elastic Property		B3LYP	B3LYP-D
Young's Modulus, E (GPa)	E_{max}	15.15	14.81
	E_{min}	2.96	3.05
	$A_E = E_{max}/E_{min}$	5.12	4.86
Shear Modulus, G (GPa)	G_{max}	5.40	5.27
	G_{min}	1.00	1.03
	$A_G = G_{max}/G_{min}$	5.40	5.12
Linear Compressibility, β (TPa^{-1})	β	12.63	12.74
Poisson's Ratio, ν	ν_{max}	1.21	1.19
	ν_{min}	-0.31	-0.28
Zener Anisotropy, A		5.41	5.11
Acoustic Modes, (km s^{-1})	max	6.18	6.14
	min	5.62	5.59

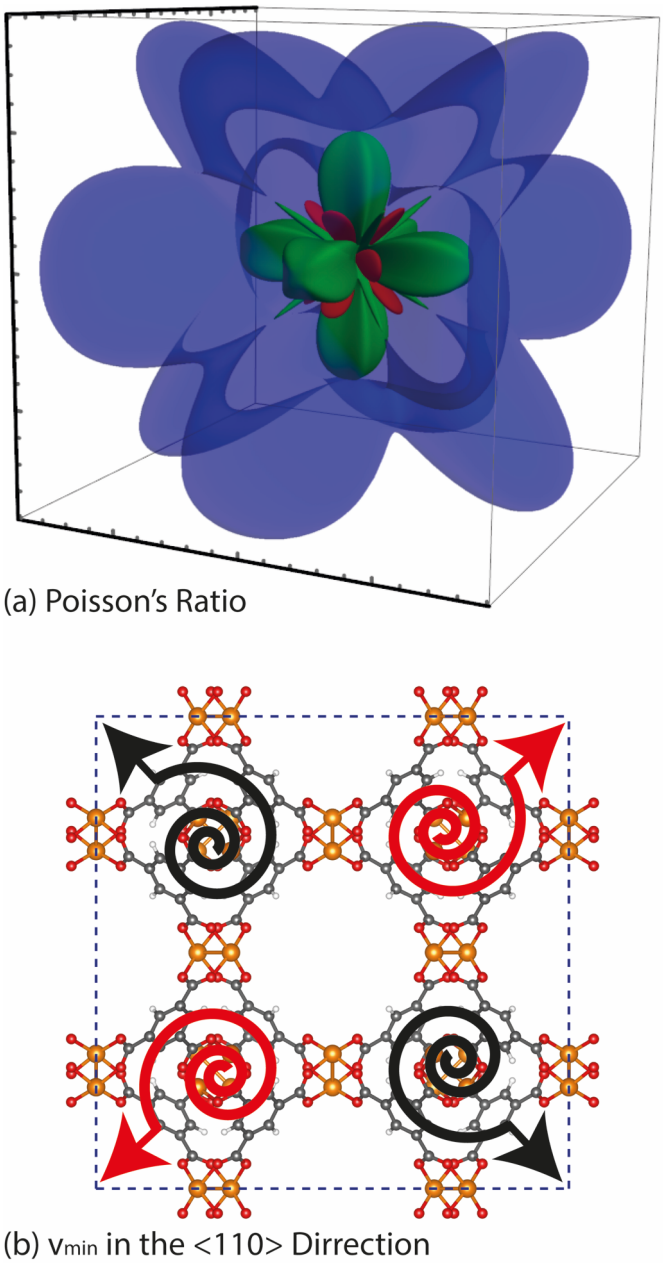

Fig. 7 Poisson's ratio representation surface *ν(ϑ, φ, χ)*, where blue signifies the maximum Poisson's ratio and green and red denote the positive and negative minimum Poisson's ratios respectively. (b) Demonstration of the mechanism responsible for the auxetic response.

β is calculated to be 12.74 TPa^{-1} at the B3LYP-D level of theory using the following equation:

$$\beta(\mathbf{u}) = u_i u_j S_{ijkl}$$

3.6 Auxetic behaviour and Poisson's ratio (ν)

An interesting elastic property of HKUST-1 is the Poisson's ratio, where in certain crystalline directions a negative value has been predicted, indicating an auxetic response. As per the shear modulus discussed before, the Poisson's ratio depends on two unit vectors (**u**, **v**) and hence the 3-D representation (Fig. 7) is again limited to the maxima and minima in each direction. This instance however, due to the auxetic directions, the maximum is depicted as blue and minimum as green and red for positive and negative values, respectively. The value of the Poisson's ratio represents the ratio of the transverse strain to the axial strain under uniaxial deformation and is obtained from the following equation:

$$\nu(\mathbf{u}, \mathbf{v}) = -\frac{u_i u_j v_k v_l S_{ijkl}}{u_i u_j u_k u_l S_{ijkl}}$$

The minima values, ν_{min} and the auxetic response of -0.3, are located in the [110] direction, with the corresponding transverse in the [1-10] direction. The mechanism behind this particular response is non-trivial to explain but could be linked to the dynamics of the inorganic-organic clusters highlighted in Fig. 5, rotating upon being stretched to allow for the elongation in the transverse direction instead of the intuitive and more common response of contraction. The suggested mechanism shows the complex nature of the origins for anomalous elastic behaviour in MOFs, as new candidates for mechanical metamaterials.[49] This is also a good example of why these particular calculations and studies are vital to obtain an accurate structure-property relationship at the atomic level between the framework in question and highlighting the complex 3-D directionally dependence elastic properties.

TABLE 3. Isotropic Voigt-Reuss-Hill (VRH) averaged elastic properties, corresponding to the polycrystalline state. The bulk (*K*), Young's (*E*) and shear (*G*) moduli are in GPa and the Poisson's ratio (ν) is dimensionless.

Functional	K_{VRH}	E_{VRH}	G_{VRH}	ν_{VRH}
B3LYP	26.39	8.10	2.80	0.45
B3LYP-D	26.16	8.07	2.78	0.45

3.7 Bulk modulus and polycrystalline mechanical properties

The stability under uniform hydrostatic compression of a given material can be quantified by the bulk modulus (*K*). In this work, we used the Voigt-Reuss-Hill (VRH) average as the theoretical value of the bulk modulus, which equates to the numerical average of the Voigt and Reuss methods that assume a uniform strain, and uniform stress respectively. The value obtained at the B3LYP level of theory was 26 GPa, which is in reasonable agreement with the literature.[50] However, as the calculated values are based on ideal polycrystalline materials assuming no residual solvent or defects, it is logical to expect experimental values would be relatively higher.

The other VRH averaged polycrystalline properties (Table 3) are the isotropic analogues of the mechanical response discussed above but with the added benefit of replicating more realistically the conditions of bulk materials used for many potential applications. For example, the values can be helpful to approximate the elastic properties of randomly oriented polycrystalline MOF coatings.[15, 51] We established that the polycrystalline average Poisson's ratio of HKUST-1 is positive

(ν_{VRH} = 0.45) despite exhibiting a significant degree of auxeticity (ν_{min} = -0.28) in single crystal form.

4. Conclusions

We demonstrated the connections that can be made between vibrational modes of a framework material and its mechanical properties. *Ab initio* density functional theory (DFT) was employed to calculate and explain the important vibrational motions, structural dynamics and elastic properties of HKUST-1. Importantly, the vibrational calculations provide insights into significant vibrational modes including 'trampoline-like' motions, paddle-wheel rotors, soft modes[32, 52] linked to symmetric collective mechanisms, which could explain the origin of auxeticity and negative thermal expansion (NTE) of HKUST-1 evidenced in certain crystallographic directions. In addition to the negative Poisson's ratio, a full analysis of the elastic properties was demonstrated explaining the structure-property relationships underlying the mechanics of the Cu-based MOF. Our theoretical approach coupled with experimental spectroscopy provide new understandings of the basic molecular mechanisms underlying lattice dynamics surrounding the elastic (in)stability of the paddle-wheel based framework material. To summarise, our findings highlight that many of the mechanical mechanisms behind the anomalous elasticity of MOF materials are yet to be fully understood. In particular, we hope that further experimental studies will be performed on HKUST-1 to confirm the level of anisotropy, with regards to the DFT predicted directional dependant Young's modulus, shear modulus and Poisson's ratio.

Acknowledgements

M. R. R. would like to thank the UK Engineering and Physical Sciences Research Council (EPSRC) for a DTA postgraduate scholarship and also an additional scholarship from the Science and Technology Facilities Council (STFC) CMSD Award 13-05. We thank Dr. B. Van de Voorde, KU Leuven for provision of sample. The authors would like to acknowledge the use of the University of Oxford Advanced Research Computing (ARC) facility in carrying out this work (http://dx.doi.org/10.5281/zenodo.22558). We are also grateful to the SCARF cluster at the Rutherford Appleton Laboratory for provision of additional computing resources.

References

1. H. C. Zhou, J. R. Long and O. M. Yaghi, *Chem. Rev.*, 2012, **112**, 673-674, J. C. Tan and B. Civalleri, *CrystEngComm*, 2015, **17**, 197-198.
2. A. K. Cheetham, C. N. Rao and R. K. Feller, *Chem. Commun.*, 2006, 4780-4795, M. O'Keeffe and O. M. Yaghi, *Chem. Rev.*, 2012, **112**, 675-702.
3. G. Ferey, *Chem. Soc. Rev.*, 2008, **37**, 191-214, A. G. Slater and A. I. Cooper, *Science*, 2015, **348**, aaa8075, H. Furukawa, K. E. Cordova, M. O'Keeffe and O. M. Yaghi, *Science*, 2013, **341**, 1230444.
4. J. Caro, *Current Opinion in Chemical Engineering*, 2011, **1**, 77-83, P. Silva, S. M. Vilela, J. P. Tome and F. A. Almeida Paz, *Chem. Soc. Rev.*, 2015, **44**, 6774-6803, M. R. Ryder and J. C. Tan, *Mater. Sci. Tech.*, 2014, **30**, 1598-1612, M. Gaab, N. Trukhan, S. Maurer, R. Gummaraju and U. Müller, *Microporous Mesoporous Mat.*, 2012, **157**, 131-136.
5. K. Sumida, D. L. Rogow, J. A. Mason, T. M. McDonald, E. D. Bloch, Z. R. Herm, T. H. Bae and J. R. Long, *Chem. Rev.*, 2012, **112**, 724-781, M. P. Suh, H. J. Park, T. K. Prasad and D. W. Lim, *Chem. Rev.*, 2012, **112**, 782-835.
6. V. Stavila, A. A. Talin and M. D. Allendorf, *Chem. Soc. Rev.*, 2014, **43**, 5994-6010.
7. Y. Cui, Y. Yue, G. Qian and B. Chen, *Chem. Rev.*, 2012, **112**, 1126-1162.
8. P. Horcajada, R. Gref, T. Baati, P. K. Allan, G. Maurin, P. Couvreur, G. Ferey, R. E. Morris and C. Serre, *Chem. Rev.*, 2012, **112**, 1232-1268, W. Cai, C. C. Chu, G. Liu and Y. X. Wang, *Small*, 2015, **11**, 4806-4822.
9. A. H. Chughtai, N. Ahmad, H. A. Younus, A. Laypkov and F. Verpoort, *Chem. Soc. Rev.*, 2015, **44**, 6804-6849.
10. L. E. Kreno, K. Leong, O. K. Farha, M. Allendorf, R. P. Van Duyne and J. T. Hupp, *Chem. Rev.*, 2012, **112**, 1105-1125, A. K. Chaudhari, I. Han and J. C. Tan, *Adv. Mater.*, 2015, **27**, 4438-4446, I. Stassen, M. Styles, T. Van Assche, N. Campagnol, J. Fransaer, J. Denayer, J. C. Tan, P. Falcaro, D. De Vos and R. Ameloot, *Chem. Mater.*, 2015, **27**, 1801-1807.
11. J. C. Tan and A. K. Cheetham, *Chem. Soc. Rev.*, 2011, **40**, 1059-1080.
12. W. Li, S. Henke and A. K. Cheetham, *APL Materials*, 2014, **2**, 123902.
13. J. C. Tan, B. Civalleri, A. Erba and E. Albanese, *Crystengcomm*, 2015, **17**, 375-382.
14. E. M. Mahdi and J.-C. Tan, *J. Membr. Sci.*, 2016, **498**, 276-290, N. W. Khun, E. M. Mahdi, S. Q. Ying, T. Sui, A. M. Korsunsky and J. C. Tan, *APL Materials*, 2014, **2**, 124101, B. Van de Voorde, I. Stassen, B. Bueken, F. Vermoortele, D. De Vos, R. Ameloot, J.-C. Tan and T. D. Bennett, *J. Mater. Chem. A*, 2015, **3**, 1737-1742.
15. I. Buchan, M. R. Ryder and J. C. Tan, *Cryst. Growth Des.*, 2015, **15**, 1991-1999, B. Van de Voorde, R. Ameloot, I. Stassen, M. Everaert, D. De Vos and J.-C. Tan, *J. Mater. Chem. B*, 2013, **1**, 7716.
16. M. D. Allendorf and V. Stavila, *CrystEngComm*, 2015, **17**, 229-246.
17. D. Bazer-Bachi, L. Assié, V. Lecocq, B. Harbuzaru and V. Falk, *Powder Technol.*, 2014, **255**, 52-59.
18. M. R. Ryder and J. C. Tan, *Dalton Trans.*, 2016, **(In Press) DOI: 10.1039/C5DT03514G**.
19. J. M. Ogborn, I. E. Collings, S. A. Moggach, A. L. Thompson and A. L. Goodwin, *Chem. Sci.*, 2012, **3**, 3011.
20. S. C. McKellar and S. A. Moggach, *Acta Crystallographica Section B Structural Science, Crystal Engineering and Materials*, 2015, **71**, A. J. Graham, J. C. Tan, D. R. Allan and S. A. Moggach, *Chem. Commun.*, 2012, **48**, 1535-1537, P. Zhao, T. D. Bennett, N. P. Casati, G. I. Lampronti, S. A. Moggach and S. A. Redfern, *Dalton Trans.*, 2015, DOI: 10.1039/c4dt02680b.
21. P. Serra-Crespo, A. Dikhtiarenko, E. Stavitski, J. Juan-Alcaniz, F. Kapteijn, F. X. Coudert and J. Gascon, *CrystEngComm*, 2015, **17**, 276-280.
22. J. C. Tan, T. D. Bennett and A. K. Cheetham, *Proc Natl Acad Sci U S A*, 2010, **107**, 9938-9943, W. Li, A. Thirumurugan, P. T. Barton, Z. Lin, S. Henke, H. H. Yeung, M. T. Wharmby, E. G. Bithell, C. J. Howard and A. K. Cheetham, *J. Am. Chem. Soc.*, 2014, DOI: 10.1021/ja500618z, J. C. Tan, P. Jain and A. K. Cheetham, *Dalton Trans.*, 2012, **41**, 3949-3952.

23. S. Henke, W. Li and A. K. Cheetham, *Chem. Sci.*, 2014, **5**, 2392-2397.
24. R. J. Marshall, S. L. Griffin, C. Wilson and R. S. Forgan, *J. Am. Chem. Soc.*, 2015, **137**, 9527-9530.
25. G. Ferey and C. Serre, *Chem. Soc. Rev.*, 2009, **38**, 1380-1399.
26. J. N. Grima and R. Caruana-Gauci, *Nat. Mater.*, 2012, **11**, 565-566.
27. A. U. Ortiz, A. Boutin, A. H. Fuchs and F.-X. Coudert, *Phys. Rev. Lett.*, 2012, **109**, 195502-195505, J. C. Tan, J. D. Furman and A. K. Cheetham, *J. Am. Chem. Soc.*, 2009, **131**, 14252-14254.
28. J. C. Tan, B. Civalleri, C. C. Lin, L. Valenzano, R. Galvelis, P. F. Chen, T. D. Bennett, C. Mellot-Draznieks, C. M. Zicovich-Wilson and A. K. Cheetham, *Phys. Rev. Lett.*, 2012, **108**, 095502, T. D. Bennett, J. Sotelo, J. C. Tan and S. A. Moggach, *CrystEngComm*, 2015, **17**, 286-289, W. Zhou, H. Wu and T. Yildirim, *Chem. Phys. Lett.*, 2010, **499**, 103-107.
29. K. Banlusan, E. Antillon and A. Strachan, *J. Phys. Chem. C*, 2015, DOI: 10.1021/acs.jpcc.5b05446, V. Ishwar Hegde, J.-C. Tan, U. V. Waghmare and A. K. Cheetham, *J. Phys. Chem. Lett.*, 2013, DOI: 10.1021/jz4016734, In Press.
30. T. D. Bennett, P. J. Saines, D. A. Keen, J. C. Tan and A. K. Cheetham, *Chem. Eur. J.*, 2013, **19**, 7049-7055, T. D. Bennett, J. C. Tan, Y. Yue, E. Baxter, C. Ducati, N. J. Terrill, H. H. M. Yeung, Z. Zhou, W. Chen, S. Henke, A. K. Cheetham and G. N. Greaves, *Nat. Commun.*, 2015, **6**, 8079.
31. G. N. Greaves, F. Meneau, O. Majerus, D. G. Jones and J. Taylor, *Science*, 2005, **308**, 1299-1302.
32. M. R. Ryder, B. Civalleri, T. D. Bennett, S. Henke, S. Rudić, G. Cinque, F. Fernandez-Alonso and J. C. Tan, *Phys. Rev. Lett.*, 2014, **113**, 215502.
33. J. Nishida, A. Tamimi, H. Fei, S. Pullen, S. Ott, S. M. Cohen and M. D. Fayer, *Proc. Natl. Acad. Sci. USA*, 2014, **111**, 18442-18447, N. Lock, M. Christensen, Y. Wu, V. K. Peterson, M. K. Thomsen, R. O. Piltz, A. J. Ramirez-Cuesta, G. J. McIntyre, K. Noren, R. Kutteh, C. J. Kepert, G. J. Kearley and B. B. Iversen, *Dalton Trans.*, 2013, **42**, 1996-2007, W. Zhou and T. Yildirim, *Phys. Rev. B*, 2006, **74**, -.
34. S. S. Chui, S. M. Lo, J. P. Charmant, A. G. Orpen and I. D. Williams, *Science*, 1999, **283**, 1148-1150.
35. R. Dovesi, R. Orlando, A. Erba, C. M. Zicovich-Wilson, B. Civalleri, S. Casassa, L. Maschio, M. Ferrabone, M. De La Pierre, P. D'Arco, Y. Noël, M. Causà, M. Rérat and B. Kirtman, *Int. J. Quantum Chem.*, 2014, **114**, 1287-1317.
36. W. F. Perger, J. Criswell, B. Civalleri and R. Dovesi, *Comput. Phys. Commun.*, 2009, **180**, 1753-1759.
37. J. F. Nye, *Physical Properties of Crystals - Chapter 8: Elasticity. Forth-Rank Tensors*, 1957.
38. Wolfram Research Inc., *Journal*, 2015.
39. A. Marmier, Z. A. D. Lethbridge, R. I. Walton, C. W. Smith, S. C. Parker and K. E. Evans, *Comput. Phys. Commun.*, 2010, **181**, 2102-2115.
40. B. Civalleri, F. Napoli, Y. Noel, C. Roetti and R. Dovesi, *CrystEngComm*, 2006, **8**, 364-371.
41. R. Dovesi, V. R. Saunders, C. Roetti, R. Orlando, C. M. Zicovich-Wilson, F. Pascale, B. Civalleri, K. Doll, N. M. Harrison, I. J. Bush, P. D'Arco and M. Llunell, *Journal*, 2014.
42. M. Ferrero, M. Rérat, R. Orlando and R. Dovesi, *The Journal of Chemical Physics*, 2008, **128**, 014110.
43. A. Comotti, S. Bracco, T. Ben, S. L. Qiu and P. Sozzani, *Angew. Chem. Int. Ed.*, 2014, **53**, 1043-1047.
44. Y. Wu, A. Kobayashi, G. J. Halder, V. K. Peterson, K. W. Chapman, N. Lock, P. D. Southon and C. J. Kepert, *Angew. Chem. Int. Ed.*, 2008, **47**, 8929-8932.
45. A. Buonaugurio, J. Graham, A. Buytendyk, K. H. Bowen, M. R. Ryder, Z. G. Keolopile, M. Haranczyk and M. Gutowski, *J. Chem. Phys.*, 2014, **140**, 221103.
46. L. H. Rimmer, M. T. Dove, A. L. Goodwin and D. C. Palmer, *Phys. Chem. Chem. Phys.*, 2014, DOI: 10.1039/c4cp01701c.
47. M. Peplow, *Nature*, 2015, **525**, 18-21.
48. V. N. Vukotic, C. A. O'Keefe, K. Zhu, K. J. Harris, C. To, R. W. Schurko and S. J. Loeb, *J. Am. Chem. Soc.*, 2015, **137**, 9643-9651, A. Comotti, S. Bracco, P. Valsesia, M. Beretta and P. Sozzani, *Angew Chem Int Ed Engl*, 2010, **49**, 1760-1764, M. Inukai, T. Fukushima, Y. Hijikata, N. Ogiwara, S. Horike and S. Kitagawa, *J. Am. Chem. Soc.*, 2015, **137**, 12183-12186.
49. L. R. Meza, A. J. Zelhofer, N. Clarke, A. J. Mateos, D. M. Kochmann and J. R. Greer, *Proc. Natl. Acad. Sci. USA*, 2015, **112**, 11502-11507, R. Gatt, L. Mizzi, J. I. Azzopardi, K. M. Azzopardi, D. Attard, A. Casha, J. Briffa and J. N. Grima, *Sci. Rep.*, 2015, **5**, 8395.
50. K. W. Chapman, G. J. Halder and P. J. Chupas, *J. Am. Chem. Soc.*, 2008, **130**, 10524-10526.
51. A. Betard and R. A. Fischer, *Chem. Rev.*, 2012, **112**, 1055-1083.
52. P. A. Fleury, *Annu. Rev. Mater. Sci.*, 1976, **6**, 157-180.